Supplementary Information

Title: **POSS/PVTMS Aerogels for Passive Cooling and THz Communication *via* Cross-linking Density Regulation and Nanoscale Bimodal Design**

Haoyu Ma[1,2,3], Maryam Fashandi[2], Zeineb Ben Rejeb[2], Piyapong Buahom[2], Jianxiang Zhao[2], Pengjian Gong[1], Qiwu Shi[4], Guangxian Li[1], and Chul B. Park[1,2*]*

1. College of Polymer Science and Engineering, State Key Laboratory of Polymer Materials Engineering, Sichuan University, 24 Yihuan Road, Nanyiduan, Chengdu, Sichuan, People's Republic of China, 610065
2. Microcellular Plastics Manufacturing Laboratory, Department of Mechanical and Industrial Engineering, University of Toronto, 5 King's College Road, Toronto, Ontario, Canada, M5S 3G8
3. Jiangsu JITRI Advanced Polymer Materials Research Institute, Tengfei Building, 88 Jiangmiao Road, Jiangbei New District, Nanjing, Jiangsu, People's Republic of China, 211800
4. College of Materials Science and Engineering, Sichuan University, 24 Yihuan Road, Nanyiduan, Chengdu, Sichuan, People's Republic of China, 610065

* Corresponding Authors:

Chul B. Park. (park@mie.utoronto.ca), Guangxian Li (guangxianli@scu.edu.cn)

1. Characterization

1.1 SEM large pore size

SEM micrographs were processed using *ImageJ* to obtain the number of large pores ($N_{SEM\_cross-section}$) and the area of i^{th} cells (A_{i_SEM}). Then, the average pore size, d_{SEM} , was obtained as follows[1]:

$$N_{SEM\_cross-section} \times \pi \left(\frac{d_{SEM}}{2} \right)^2 = \sum_{i=1}^{N_{SEM\_cross-section}} A_{i\_SEM} \quad \text{(S1)}$$

1.2 SEM large pore density

The number of cells ($N_{SEM\_cross\text{-}section}$, *unit: #/cm²*) in a certain area ($A_{SEM\_cross\text{-}section}$, *unit: cm²*) was counted based on SEM micrographs. *N/A* then represents the cell density at the cross-section. In order to transfer to 3D cell density, 3/2 power is commonly applied on (*N/A*) and the corresponding unit becomes *#/cm³*.[1]

$$n_{SEM} = \left(\frac{N_{SEM\_cross-section}}{A_{SEM\_cross-section}} \right)^{3/2} \quad \text{(S2)}$$

1.3 Void fraction

The density was calculated by measuring the weight and the volume of the samples. and the void fraction (*V*) was calculated by following:

$$V = (1 - \rho_A / \rho_S) \times 100\% \quad \text{(S3)}$$

1.4 mm-wave transmission

PNA-X network analyzer (Keysight N5232B) were used to characterize the dielectric permittivity and dielectric loss of the aerogel in *Ku*-band (12.4–18.0 GHz). The waveguide method (Keysight N5232B) was used to test the electromagnetic wave transmittance of aerogel materials (4 mm thickness) in the *Ku*-band. The transmission ratio (*T*) was calculated as follows [2]:

$$T = 10^{(S_{21s} - S_{21g})/10} \quad \text{(S4)}$$

where S_{21s} and S_{21g} are the coefficient of transmission (also known as the S parameter) for the test with and without the sample, respectively.

1.5 Thermal conductivity

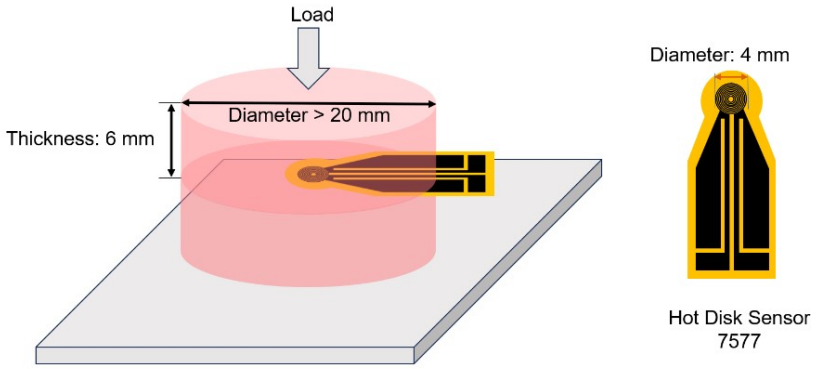

Figure S1. Thermal insulation property test.

A hot-disk transient plane source thermal (TPS) constant analyzer model 2500 S (Hot Disk) was used for the transient isotropic measurements. The thermal conductivity measurement was carried out at room temperature (25 ◦C) by stacking samples two by two (thickness: 6 mm, diameter: 20-25 mm). A disk shaped TPS Kapton-sensor (7577) with a diameter of 4 mm was used in all measurements. The sensor was placed between the two stacks of samples.

2. Hydrophilic property and solar reflectivity

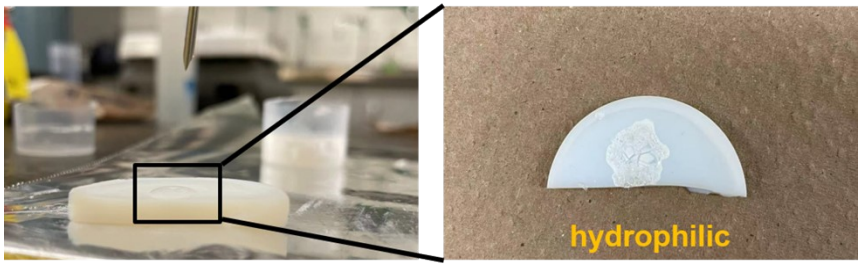

Figure S2. Hydrophilic property of PVTMS aerogel;

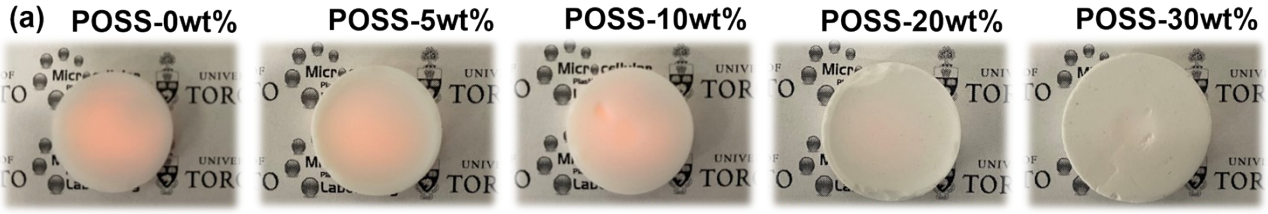

Figure S3. Digital micrographs of pristine PVTMS aerogel and POSS@PVTMS nano-aerogel at various POSS contents covered on the light source;

Figure S3 shows digital micrographs of POSS@PVTMS aerogels with various POSS content covered on the light source. The light transmission property gradually decreases when the POSS content increases.

3. FDTD Simulation

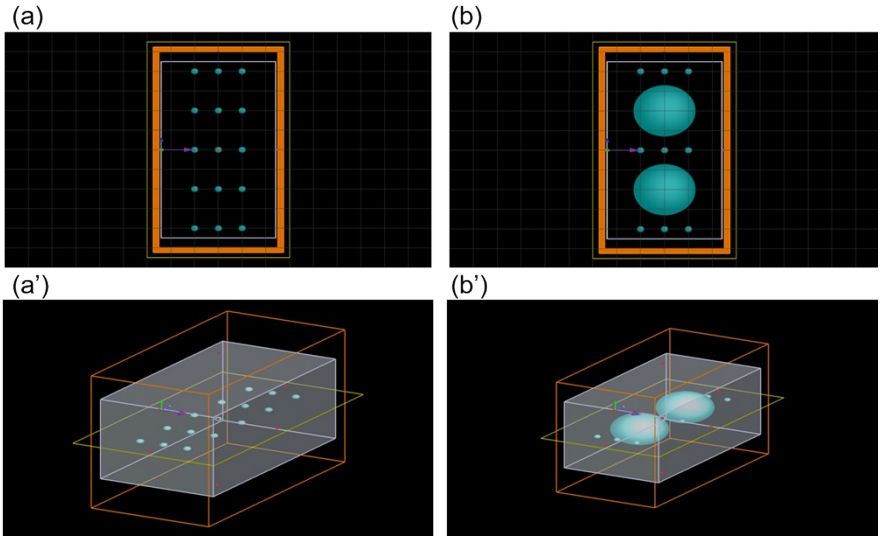

Figure S4. 2D and 3D FDTD models for unimodal (a-a') and bimodal (b-b') aerogel pore system.

During the model construction, 30 nm pores were constructed in a unimodal system, and both 30 nm and 260 nm pores were constructed in a bimodal system. The simulated wavelength ranges from 200-700 nm.

4. Property

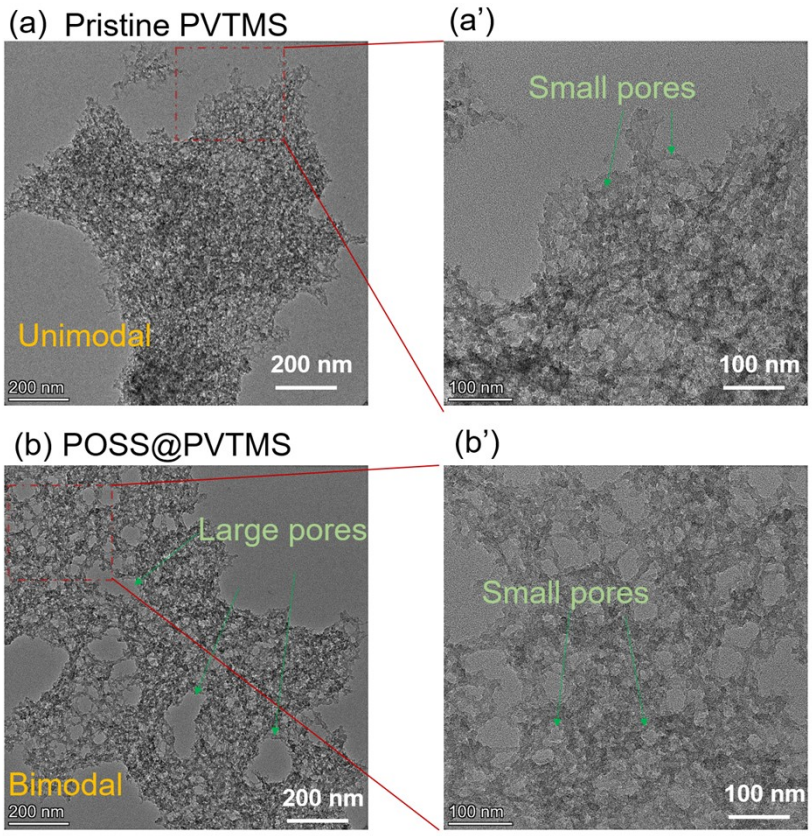

Figure S5. TEM micrographs of (a) pristine PVTMS aerogel and (b) POSS@PVTMS-20wt.% aerogel;

As **Figure S5** shows, high resolution TEM was used to further confirm the bimodal porous structure of the aerogel. As **Figure S5** (b) shows, it can also be found that larger pores (~200 nm) generated in small pores (30-80 nm) by adding POSS nanofiller.

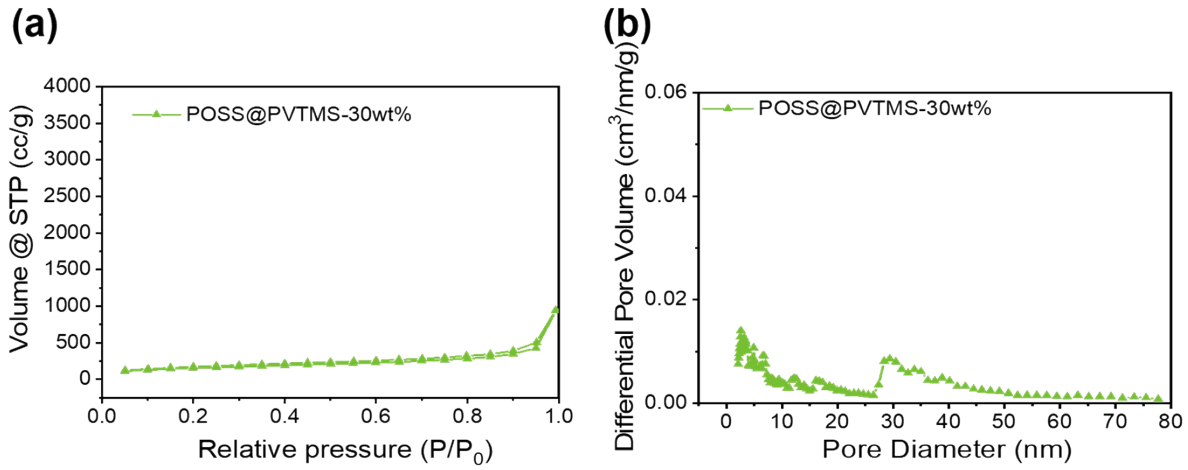

Figure S6. (a) Nitrogen adsorption-desorption isotherms and (b) pore diameter distribution curves of POSS@PVTMS-30wt.% aerogel.

The pore shapes and types were investigated based on IUPAC's technical report on the physisorption of gases using nitrogen adsorption-desorption analysis [3, 4]. For POSS@PVTMS-30 wt.% aerogel, adding too high a content of POSS nanofiller significantly decreased the cross-linking density of the PVTMS molecular chain, thereby, deteriorating the mesoporous structure, as indicated by the reduced pore volume fraction of ~30 nm pores.

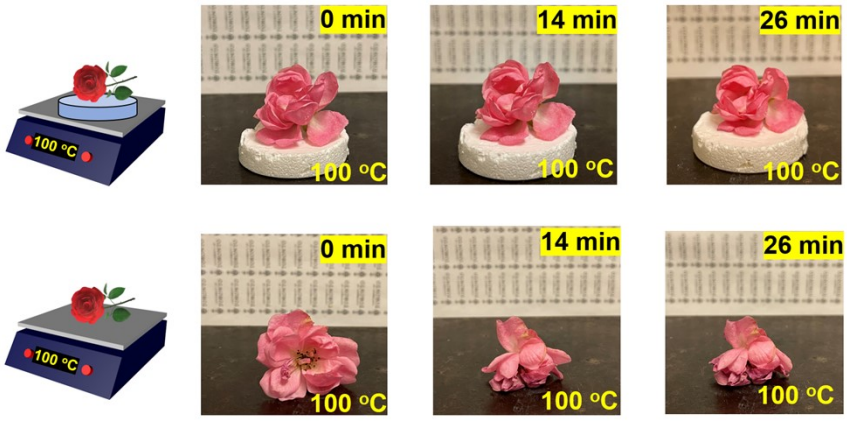

Figure S7. Thermal insulation effect on the water evaporation process of a flower over time;

Figure S7 shows the effect of aerogel on the water evaporation process of a flower placed on the hot plate with and without an interposed insulating aerogel. Without the aerogel, water in the flower evaporates, and the flower begins to limp because of water loss over time. On the other hand, when the aerogel is used as an insulation layer, the aerogel could effectively block heat transfer from the hot plate and, hence, prevent the water evaporation process from preserving the flower on the aerogel's upper surface.

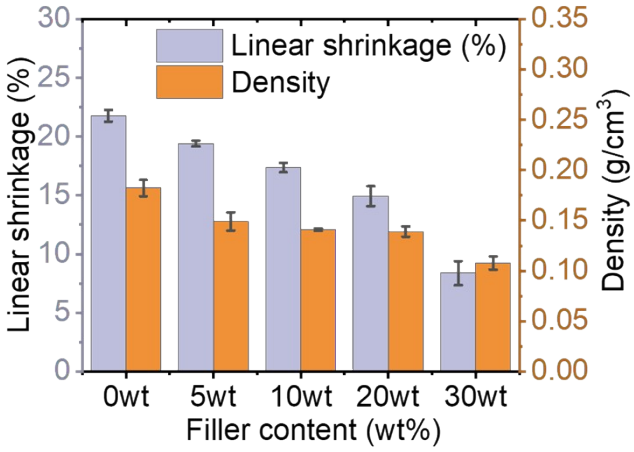

Figure S8. Linear shrinkage and density of POSS@PVTMS aerogel with various POSS content

Figure S8 shows line shrinkage and density of POSS@PVTMS aerogel with various nanofiller content, it is noted that the degree of aerogel shrinkage decreased with increasing POSS content after $scCO_2$ drying. Meanwhile, the density of nano-aerogel also slightly decreased with increasing POSS nanofiller content.

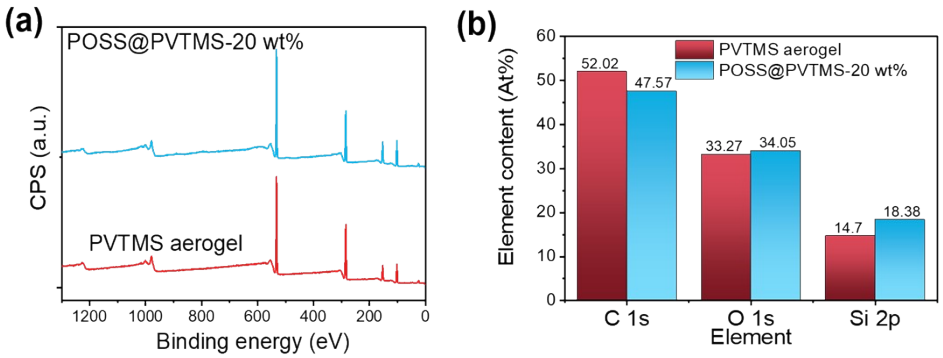

Figure S9. (a) Broadband XPS spectra and (b) Carbon, oxygen and silicon element contents;

Figure S9 a-b show the element contents of the POSS@PVTMS-20wt% aerogel with the pristine PVTMS aerogel, which were obtained from the XPS spectra in **Figure S9 a**. It was found that the content of carbon (C 1s) in the POSS@PVTMS aerogel decreased from that in the pristine PVTMS aerogel by 8.6%, whereas the contents of oxygen (O 1s) and silicon (Si 2p) increased by 2.3% and 25.0%, respectively.

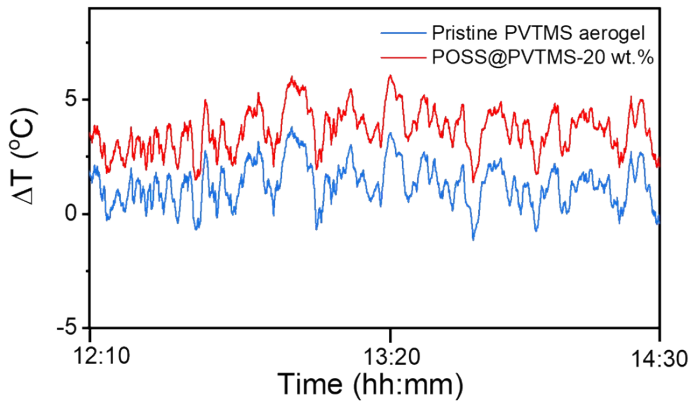

Figure S10. Temperature difference for pristine PVTMS and POSS@PVTMS aerogel cooler

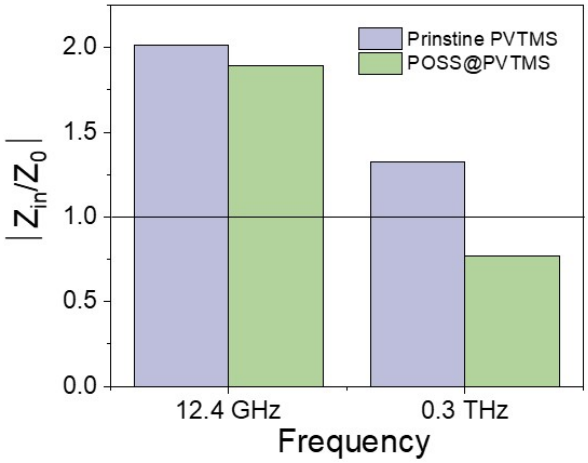

Figure S11. Impedance matching of pristine PVTMS aerogel and POSS@PVTMS aerogel at GHz and THz.

As shown in **Figure S11**, the impedance matching (Z_{in}/Z_0) data was characterized and calculated using equation 1 (manuscript). It is noted that, compare to pristine PVTMS aerogel, the impedance match (Z_{in}/Z_0) of POSS@PVTMS aerogel closer to 1, which mean impedance difference decreased by adding POSS nanofiller. The decreased impedance match was beneficial for decreasing the electromagnetic wave reflection and enhancing the transmission both in GHz (12.4-18GHz) and THz (0.3-1 THz).

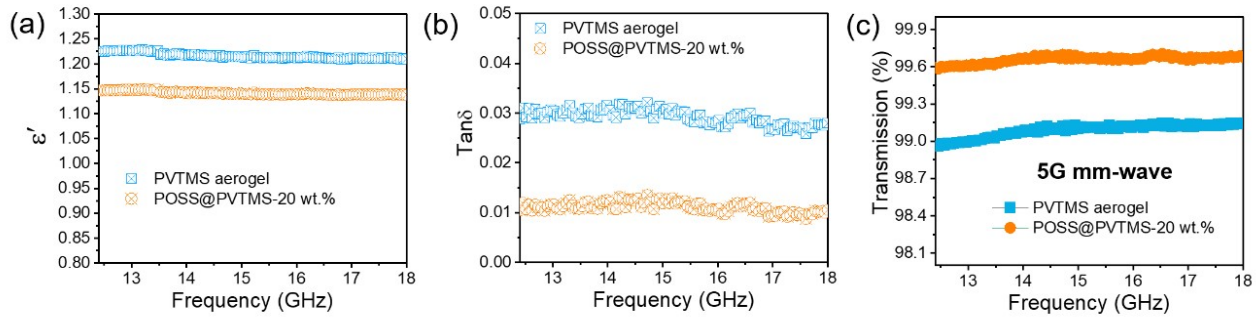

Figure S12. (a) Dielectric permittivity and (b) dielectric loss at *Ku*-band frequency ranges of pristine PVTMS and POSS@PVTMS-20wt.% aerogels; (c) The *Ku*-band electromagnetic wave transmissions (4 mm thickness);

Figure S12a-b show the dielectric permittivity D_k and dielectric loss D_f of pristine PVTMS and POSS@PVTMS-20wt.% aerogels in *Ku*-band frequency (12.4–18.0 GHz) ranges. With the addition of POSS nanofillers, the dielectric permittivity and dielectric loss all decreased. As **Figure S12c** shows, mm-wave transmittance of POSS@PVTMS-20 wt.% also increased by adding POSS nanofiller, and the average mm-wave transmittance of POSS@PVTMS in the *Ku* band reached 99.7%.

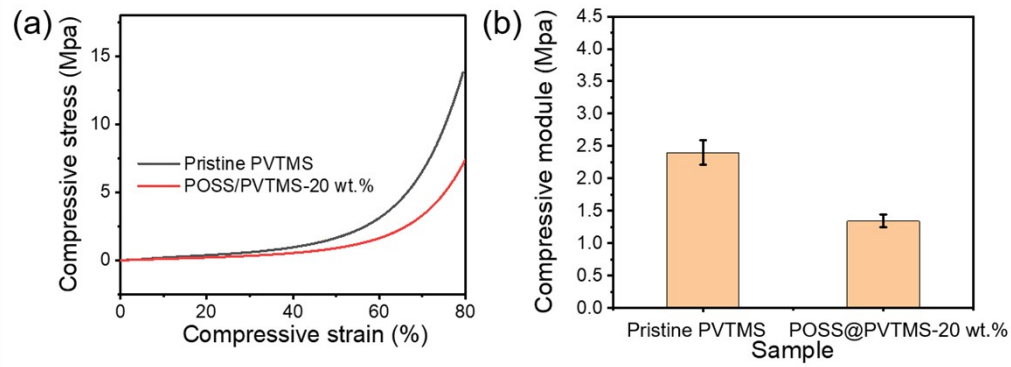

Figure S13. (a) Stress-strain curve and (b) compressive modulus of pristine PVTMS and POSS@PVTMS-20wt.% aerogel.

As shown in **Figure S13**, the compressive mechanical performance of pristine PVTMS and POSS@PVTMS-20wt.% aerogel was characterized. It is found that the compressive module decreased by adding POSS nanofiller. The decreased compressive module could be ascribed to two proposed reasons: 1) the cross-linking density decreased by adding POSS nanofiller; 2) The void

fraction increased for POSS@PVTMS-20wt.% compare to pristine PVTMS aerogel.

Reference

1. H. Ma, P. Gong, S. Zhai, Y. Huang, Y. Niu, C. B. Park and G. Li, *Chem. Eng. Sci.*, 2019, **207**, 892-902.
2. L. Zhang, D. Chen, B. Jin, B. Zhang, P. Gong, B. Zhang, C. B. Park and G. Li, *Ind. Eng. Chem. Res.*, 2023, **62**, 5850-5863.
3. M. Thommes, K. Kaneko, A. V. Neimark, J. P. Olivier, F. Rodriguez-Reinoso, J. Rouquerol and K. S. W. Sing, *Pure Appl. Chem.*, 2015, **87**, 1051-1069.
4. M. Fashandi, S. Karamikamkar, S. N. Leung, H. E. Naguib, J. Hong, B. Liang and C. B. Park, *J. Colloid Interface Sci.*, 2022, **608**, 720-734.